RSC Advances

Cite this: *RSC Advances*, 2012, **2**, 9437–9442

www.rsc.org/advances

PAPER

Cytotoxicity and slow release of the anti-cancer drug doxorubicin from ZIF-8†

Iane B. Vasconcelos,[a] Teresinha G. da Silva,[b] Gardenia C. G. Militão,[c] Thereza A. Soares,[d] Nailton M. Rodrigues,[e] Marcelo O. Rodrigues,[df] Nivan B. da Costa Jr.,[e] Ricardo O. Freire[e] and Severino A. Junior*[d]

Received 30th May 2012, Accepted 2nd August 2012
DOI: 10.1039/c2ra21087h

Metal–organic frameworks are emerging as a powerful platform for the delivery and controlled release of several drug molecules. Herein, we report the incorporation of the anti-cancer drug doxorubicin into the zeolitic imidazolate framework (ZIF-8) with high-load and progressive release. Adsorption measurements show that doxorubicin is incorporated into ZIF-8 with a load of 0.049 g doxorubicin g^{-1} dehydrated ZIF-8. Doxorubicin is released in a highly controlled and progressive fashion with 66% of the drug released after 30 days. We also characterize the antitumoral potential and cytotoxicity of the doxorubicin-ZIF-8 (DOXO-ZIF-8) complex towards the mucoepidermoid carcinoma of human lung (NCI-H292), human colorectal adenocarcinoma (HT-29), and human promyelocytic leukemia (HL-60) cell lines. It is shown that the complex doxorubicin-ZIF-8 exhibits lower cytotoxicity than pure doxorubicin for the tested cells, possibly due to the slower release of the incorporated drug. Furthermore, host–guest interactions have been addressed from a microscopic perspective through molecular docking simulations. In conjunction with our experimental characterization, the calculations suggest that doxorubicin binds preferentially to the surface rather than into the pores of ZIF-8, whose entry diameter is at least half the size of the shortest axis of the drug. These findings are also consistent with high-resolution X-ray crystallography and NMR spectroscopy studies of ZIF-8 which shows that this framework is very rigid under constant pressure in contrast to previous experimental and theoretical studies of ZIF-8 under gas pressure.

Introduction

Cancer therapies are curbed by the their unspecificity towards tumor cells, leading to high doses, rapid clearance, poor pharmacokinetics and serious side effects.[1–3] Nanoparticle-based therapeutics can alleviate many of the pitfalls associated with free drug therapeutics while improving the efficacy of conventional drugs. The clinical success of nanoparticle therapies is illustrated by the large number of nanoparticle–drug conjugates under different stages of clinical development.[2–5] Metal–organic frameworks (MOF) or coordination polymers are crystalline solids assembled by the connection of metal ions or clusters through tunable organic linkers whose structures are held together either by strong metal–ligand bonding or by weaker bonding forces (*e.g.* hydrogen bonding and π–π interactions).[6–8] The modular nature of MOFs coupled with the many different types of bridging ligands allows for a multitude of frameworks with desirable topologies, architectures, and properties inherent to the building blocks, such as geometric rigidity, chemical functionality, or chirality.[9] The versatility of MOFs has led to their broad application in gas separation and/or storage, sensors, non-linear optics, catalysis, and forensic chemistry.[10–19]

Over the past five years, a promising application for MOFs has emerged in the controlled delivery of several drug molecules.[5,20–22] These applications rely on the several desirable properties of MOFs as potential drug carriers: their remarkably high surface areas and large pore sizes for drug encapsulation, their intrinsic biodegradability, their versatile functionality for post-synthesis grafting of drug molecules, and their scalability to the nanoregime.[5,20] In particular, non-toxic porous iron(III)-based MOFs have been reported as superior nanocarriers for the controlled delivery of several antitumoral and retroviral drugs.[21,22] Another class of MOFs, the zeolitic imidazolate framework (ZIF), also exhibits interesting properties as a carrier.[23–26] ZIFs are comprised of tetrahedral transition metal ionsconnected by imidazolate units arranged in topologies with

[a]*Programa de Pós-Graduação em Ciência dos Materiais, UFPE, 50590-470, Recife-PE, Brazil*
[b]*Departamento de Antibióticos, UFPE, 50590-470, Recife-PE, Brazil*
[c]*Departamento de Fisiologia e Farmacologia, UFPE, 50590-470, Recife-PE, Brazil*
[d]*Departamento de Química Fundamental, UFPE, Av. Jornalista Aníbal Fernandes, s/n - Cidade Universitária, 50740-560, Recife-PE, Brazil. E-mail: salvesjr@ufpe.br; Fax: +55 81 21268442; Tel: +55 81 21267475*
[e]*Departamento de Química, UFS, 49100-000, São Cristóvão-SE, Brazil*
[f]*Instituto de Química, Universidade de Brasília, 70910-900, Brasília–DF, Brazil*

† Electronic Supplementary Information (ESI) available: infrared spectra, TGA/DTGA curves, and SEM analysis. See DOI: 10.1039/c2ra21087h

large cages and small apertures. ZIFs exhibit both high thermal and chemical stability, thus overcoming two of the main issues when considering the use of MOFs in biomedical applications.[23,24,26] Recently, it has been reported that ZIF-8 can function as a pH-triggered carrier for the anticancer drug 5-fluorouracil.[27]

In this report, we describe the incorporation of the antitumoral drug doxorubicin (DOXO) into ZIF-8 with high-load and controlled release *via* Fourier transform infrared (FTIR) spectroscopy, thermogravimetric analysis (TGA), X-ray diffraction (XRD), and confocal microscopy. It is further shown that the DOXO–ZIF-8 complex has a higher antitumoral potential and lower cytotoxicity towards the HL-60 and MCF-7 cell lines compared with doxorubicin in the absence of ZIF-8. Host–guest interactions were characterized from a macroscopic perspective *via* computational simulations. These simulations offer insights into the ZIF-8 binding conformation and preferences of doxorubicin, and are consistent with the powder synchrotron X-ray diffraction measurements. These findings suggest that ZIF-8 can be a potential carrier system for doxorubicin, whose short half-life and low bioavailability in biological media, coupled with low membrane permeability, presents a much improved therapeutic profile when entrapped in nanocarriers.[21,28]

Results and discussion

A high-resolution X-ray powder pattern was acquired at room temperature for DOXO–ZIF-8 (Fig. 1). The collected data could be readily indexed with the presence of one impurity line *via* DICVOL 04.[11] Due to a lack of crystallographic data for doxorubicin, the Rietveld refinement for the DOXO–ZIF-8 complex was performed considering only the atomic coordinates of the ZIF-8. The refinement of the XRD data sets shows that the structural integrity of ZIF-8 remains unaltered after adsorption of the drug. Doxorubicin in solution has a pallid orange color, which changes to purple upon its incorporation into ZIF-8, thus providing further evidence for the formation of the DOXO–ZIF-8 complex.

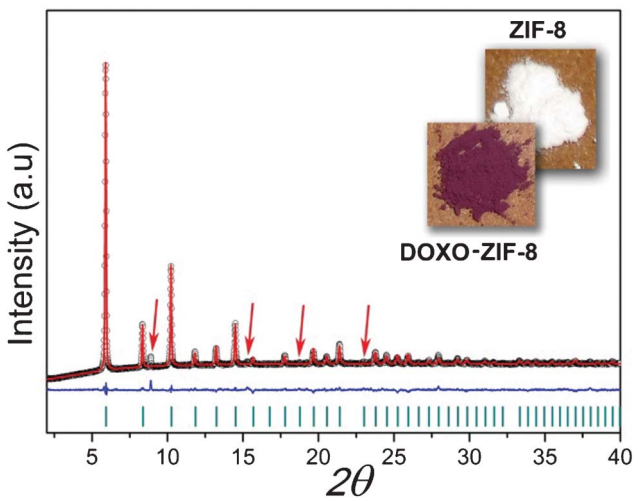

Fig. 1 Final Rietveld refinement of DOXO–ZIF-8. Observed data points are indicated as black circles, the best-fit profile (upper trace) and the difference pattern (lower trace) are drawn as solid red and blue lines, respectively. Dark cyan vertical bars and red arrows indicate the angular positions of the allowed Bragg reflections and impurity lines from lactose. Reliability factors for refinement: R_p: 1.4; R_{wp}: 2.07; χ^2: 5.28; R_F^2: 18.52.

FTIR spectra were obtained for ZIF-8, doxorubicin, and the complex DOXO–ZIF-8 (ESI†, Fig. S1). In the spectrum corresponding to ZIF-8, two bands at 3135 and 2928 cm^{-1} can be observed for the aromatic C–H stretch and the aliphatic C–H stretch of the imidazole, respectively. The 1606 cm^{-1} band is for the C–C stretch, and the peak at 1580 cm^{-1} is for the C–N stretch. The C–N absorption bands are found in the 1100–1400 cm^{-1} region. The absorption band at 421 cm^{-1} is associated with the Zn–N stretching mode. These assignments are in agreement with the FTIR measurements from Park *et al.*[29] Several bands are observed for doxorubicin: the band at 3441 cm^{-1} is due to an axial strain of the N–H bond, at 2936 cm^{-1} to C–H axial deformation, at 1635 cm^{-1} to the axial deformation of the C–O bond, and at 100–1260 cm^{-1} to the absorption associated with the stretching of the alcohol group. In the the region between 675–900 cm^{-1} there is an out-of-plane bending of the –OH group that has also been reported by Chouhan *et al.*[30] The FTIR spectrum analysis for the system DOXO–ZIF-8 does not undoubtedly show the adsorption of doxorubicin into ZIF-8, but the detection of characteristic bands for both ZIF-8 and DOXO indicates the presence of both compounds. Moreover, the incorporation of doxorubicin into ZIF-8 is supported by the color change of the ZIF-8 crystals, which were initially colorless, and after the incorporation process, exhibited a purple color.

The thermal analysis TG/DTG curve for DOXO–ZIF-8 shows four weight loss events (%) at temperature ranges of 80–100, 190–390, and 390–620 °C (ESI†, Fig. S2). The first event is related to the loss of hydration water molecules trapped in the pores of ZIF-8. The second event is typical of the loss of the DOXO molecules since the decomposition profile of ZIF-8 has not displayed any weight loss in this temperature range. The third decomposition event corresponds to the simultaneous thermal decomposition of DOXO and ZIF-8 followed by carbonization of the material. The decomposition of ZIF-8 and DOXO–ZIF-8 samples yields residual zinc oxide (ZnO) (*ca.* 37 and 21% respectively). A similar ratio between MIL-53(Cr, Fe) and MIL-53(Cr, Fe)–ibuprofen has been reported in the literature by Horcajada and co-authors.[22] The SEM image for ZIF-8 shows nanometer-sized crystals with an average diameter around 200 nm (ESI†, Fig. S3B). Comparison of this value against our XRD results indicates the formation of nanoparticle microclusters. The SEM image for DOXO–ZIF-8 shows crystalline nanoparticles with sizes of about 300 nm, which are similar to the crystallite sizes estimated by XRD (ESI†, Fig. S3C). The photomicrograph of doxorubicin is also shown in Fig. S3A to assist with data interpreting. Adsorption measurements for the system DOXO–ZIF-8 show that drug incorporation was carried out successfully with a load of 0.049 g of doxorubicin g^{-1} of dehydrated ZIF-8. This load is less than the value obtained for the 5-fluorouracil–ZIF-8 system, *i.e.* 0.660 g of 5-fluorouracil g^{-1} of ZIF-8.[27] However, given the much smaller size of 5-fluorouracil (5.42 × 4.50 × 0.00 Å) compared to doxorubicin (14.64 × 10.02 × 6.90 Å) it is likely that the former is incorporated inside the framework pores, which we argue is not the case for the latter (see below).

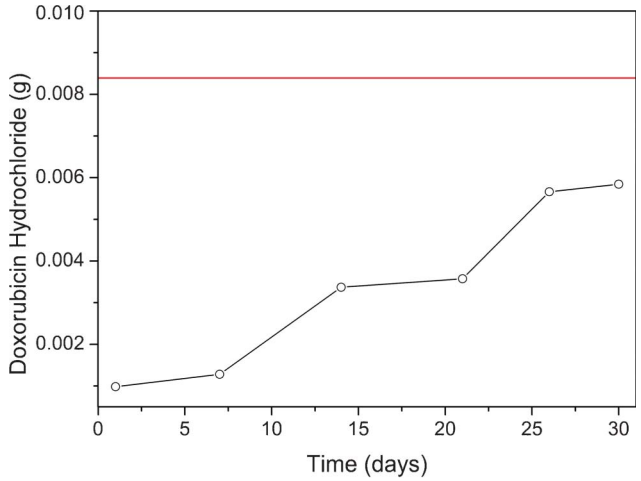

Fig. 2 Graphical representation of the amount of drug released from ZIF-8 in 30 days. The red line in the graph represents the total amount of drug incorporated into the ZIF-8.

UV-vis spectroscopy was used to measure the doxorubicin release profile based on the amount of drug in phosphate buffer at pH 7.4 (Fig. 2). ZIF-8 has been shown to be very stable in these conditions.[27] After 30 days, only 66% of the drug was released suggesting strong chemical interactions with the ZIF-8 framework. The release profile from ZIF-8 showed a pattern of zero-order, similar to the release profile previously reported for the system ibuprofen–MIL-100.[31] It has been previously shown that ibuprofen exhibits different release profiles depending on the nature of the metal present in the MOF used for adsorption. For ZIF-8 containing Zn^{2+} ions, the release profile still followed zero-order kinetics after 30 days. This is an excellent rate compared with doxorubicin release from MIL-100, which is 100% in 14 days.[21]

The cytotoxicities of ZIF-8 and the complex DOXO–ZIF-8 were assessed by the colorimetric MTT assay (Table 1). The method is based on the conversion of 3-(4,5-dimethyl-2-thiazole)-2,5-diphenyl-2*H*-tetrazolium bromide (MTT) into blue formazan from mitochondrial enzymes present only in metabolically active cells.[32] It has been used in the screening program of the National Cancer Institute of the United States (NCI), which tests more than 10 000 samples each year.[33] The MTT assay offers a fast and sensitive approach for the analysis of the viability and metabolic state of the cell. The concentrations causing 50% cell growth inhibition (IC_{50}) at three lineages ranged from 0.01 to 7.9 μg mL^{-1} for DOXO, and 0.79 to14.96 μg mL^{-1} for DOXO–ZIF-8. CNI-H292 proved to be the most sensitive lineage with an IC_{50} value of 0.01 μg mL^{-1} for DOXO and 0.79 μg mL^{-1} for DOXO–ZIF-8. ZIF-8 was not cytotoxic at the tested concentration (25 μg mL^{-1}). The reduced cytotoxicity of DOXO–ZIF-8 compared to DOXO may be explained by the slow release of the drug.

Table 1 Cytotoxic activity of doxorubicin (DOXO), ZIF-8 and DOXO–ZIF-8 system[a]

	Cell Line IC_{50} (μg mL^{-1}) (CI)		
Substances	CNI-H292	HL-60	HT-29
DOXO	0.01 (0.01–0.5)	0.03 (0.005–0.3)	7.9 (5.6–11.4)
ZIF-8	>25	>25	>25
DOXO–ZIF-8	0.79 (0.6–0.9)	5.1 (2.0–2.9)	14.96 (10.2–21.8)

[a] Data are presented as IC_{50} values and 95% confidence intervals (CIs) for NCI, HT-29 and HL-60 cell lines.

Confocal microscopy analysis showed the fluorescence pattern and intracellular fate of the DOXO and DOXO–ZIF-8 systems. The DOXO fluorescence was primarily detected in intracellular vesicles and nuclei, consistent with its intercalation within genomic DNA. The complex DOXO–ZIF-8 was dispersed in the cell. Some of DOXO–ZIF-8-treated cells presented stained-tubular processes towards the nuclear matrix (Fig. 3E, 3F, 3I, 3J). No fluorescence signal could be found in the control cells (Fig. 3A, top left) and only a weak signal could be detected in ZIF-treated cells (Fig. 3B, top right). However, cells treated with this complex showed an evident shift in the red signal when compared with DOXO alone (Fig. 3C, 3D, 3G, 3H). Both DOXO and DOXO–ZIF-8 complexes induced considerable morphological changes in HL-60 cells in a time- and dose-dependent manner, with induction of bubbles from the cellular surface resembling apoptotic bodies. Luminescent properties were more pronounced in cells treated with DOXO–ZIF-8, which may indicate that complexation with ZIF-8 facilitated the entry of doxorubicin in the cells (Fig. 3). Macromolecular pro-drugs such as doxorubicin enter cells *via* endocytosis, and are compartmentalized in the endosome and lysosome.[34] Hence, it is plausible that free and ZIF-8-complexed doxorubicin exhibit different mechanisms of entry into cells.

The experimental measurements presented in this report show that doxorubicin is loaded onto ZIF-8 and released at slow rate. Such release behavior may be interpreted as indicative of doxorubicin being incorporated into the pores. However, such a conclusion is not reconcilable with the fact that ZIF-8 has been shown by X-ray crystallography and NMR spectroscopy to be very rigid. Additionally, the largest pore size in the ZIF-8 structure has a diameter of *ca.* 11.6 Å interconnected by 6-ring windows of a diameter of 3.40 Å whereas doxorubicin has

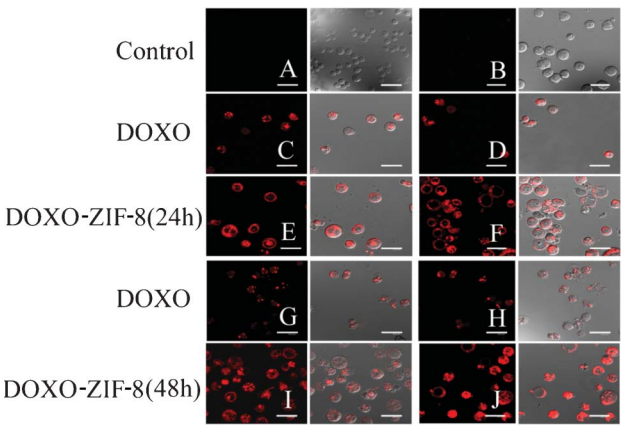

Fig. 3 Confocal microscopy of HL-60 cells incubated in the absence (A) or presence of ZIF8 (B); IC_{50} (C) and 2 × IC_{50} (D) of DOXO; IC_{50} (E) and 2 × IC_{50} (F) of DOXO–ZIF-8 for 24 h; IC_{50} (G) and 2 × IC_{50} (H) of DOXO; IC_{50} (I) and 2 × IC_{50} (J) of DOXO–ZIF-8 for 48 h. The left column represents the fluorescence of the red channel and the right column represents the merging of the red channel and the differential interference contrast image.

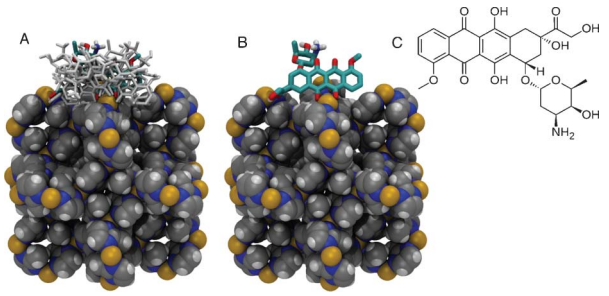

Fig. 4 Representation of the ZIF-8 (in van der Waals spheres) crystallographic unit cell and the docked conformations of doxorubicin in stick. (A) Ten lowest energy conformations of doxorubicin bound to the X-ray structure of ZIF-8. (B) The lowest energy conformation with an occurrence of *ca.* 70% among the 100 lowest energy conformers selected from a total of 1.35×10^8 sampled conformations. (C) Chemical structure of doxorubicin. Carbon atoms in grey, nitrogen in blue, hydrogen in white, and Zn^{2+} cations in yellow.

dimensions of $14.64 \times 10.02 \times 6.90$ Å, and XDR analysis of the complex shows unchanged lattice parameters for ZIF-8 previous to and after doxorubicin loading. Hence, doxorubicin appears overly large to pass through even the largest pore entrance. To ascertain such an assessment, flexible molecular docking calculations were performed for doxorubicin on the structure of ZIF-8. Could doxorubicin adsorb onto the ZIF-8 surface so effectively to explain the measured release rates?

We have addressed this question by the means of molecular docking simulations of doxorubicin onto/into the ZIF-8 structure. The treatment of doxorubicin dihedral torsions as flexible allows for different conformations of the molecule to be taken into account during the conformational sampling and binding energy calculations. A total of 1.35×10^8 conformations of doxorubicin were sampled and ranked according to their interaction energies to the ZIF-8 structure. Among the sampled conformations, the 100 lowest conformations bind exclusively only to the framework surface (Fig. 4). Doxorubicin interacts with the Zn^{2+} cations *via* chelating sites comprised of the quinone and the phenolic oxygens on both sides of the anthracycline aromatic moiety (Fig. 4). The Zn^{2+} cations in the ZIF-8 structure exhibit tetrahedral geometry coordinated by four neighboring imidazolate groups. It is expected that the Zn^{2+} cations on the surface of the ZIF-8 structure will have two imidazolate ligands replaced by water molecules. Our molecular docking results show that doxorubicin binds to the Zn^{2+} cation, thus maintaining its tetrahedral coordination geometry, possibly by replacing two water molecules acting as ligands to the cation. A similar binding pattern has been previously reported for doxorubicin complexed with Fe^{3+} cations *via* absorption and circular dichroism measurements in aqueous solution and in semi-aqueous MeOH.[34] Limiting the conformational search exclusively to the largest pore cavity did not yield conformations with favorable interaction energies. It is interesting to note that both X-ray diffraction and NMR spectroscopy structural characterization of ZIF-8 show that the framework is very rigid.[35] This is in contrast with previous theoretical and experimental studies under gas pressure, which is of great relevance for applications in gas storage.[36,37] Because such conditions are not expected in the cell, the pressure-induced flexibility of ZIF-8 should not be relevant for the present work.

Conclusions

Doxorubicin is an anthracycline antitumoral drug widely used in the treatment of various cancers. Despite its efficacy in the treatment of carcinomas, sarcomas and hematological cancers, doxorubicin exhibits serious cumulative dose-dependent cardiotoxicity. Its therapeutical efficiency is further compromised due to the drug poor stability in biological media and low membrane permeability. However, it has been shown that Zn^{2+} can competitively inhibit the binding interaction of the anthracyclines with the major contractile protein cardiac myosin, thus exerting a cardioprotective effect against the drug.[38] It has also been shown that the therapeutic profile of doxorubicin is much improved when the drug is entrapped in nanocarriers.[21,28] The use of ZIF-8 as a carrier for doxorubicin may alleviate cardiotoxic side effects while increasing its therapeutical efficiency. We have demonstrated that doxorubicin can be incorporated in ZIF-8 with a load of 0.049 g of doxorubicin g^{-1} of dehydrated ZIF-8 and a very slow release rate with a pattern of zero-order (which lasts for 30 days). We have also shown that the DOXO–ZIF-8 system is internalized by HL-60 cells, and exhibits reduced cytotoxicity compared to pure doxorubicin, likely due to its the slow release from ZIF-8. Refinement of XRD showed that the lattice parameters for ZIF-8 are unaltered after adsorption of doxorubicin, which suggests that doxorubicin interacts predominantly with the surface of ZIF-8. This assumption is supported by molecular docking calculations, which show that doxorubicin binds to the Zn^{2+} cations on the framework surface *via* quinone and phenolic oxygens on the anthracycline aromatic moiety.

Experimental and computational procedures

Chemicals. ZIF-8 was purchased from Aldrich and used without further purification. Hydrochloride doxorubicin was obtained from the Bergamo Pharmaceutical Chemistry Laboratory.

X-Ray diffraction. The powder synchrotron X-ray diffraction patterns were acquired at ambient temperature (300 K) in a 2θ range of 5–48° using a Huber diffractometer in high resolution mode (low intensity, $E = 10$ keV) in the multi-proposed powder station D10A-XRD2 beam line of the Brazilian Synchrotron Light Laboratory (LNLS). The Rietveld refinement[39] for ZIF-8 and DOXO–ZIF-8 were performed with the software GSAS/EXPGUI,[40,41] using the atomic coordinates of the structural model previously reported as a starting premise.[42] The preferential orientation was corrected using the spherical harmonic model (sixth order) proposed by Jarvinen,[43] and the peak profile was adjusted by the Thompson–Cox–Hastings function[44] modified by Young and Desai (pV-TCHZ).[45] Surface roughness correction was refined by Pitschke function[46] and background was fitted by an eighth-degree shifted Chebyshev polynomial function. In the final runs, the following parameters were refined: scale factor, background and absorption coefficients, spherical harmonic, unit-cell parameters, and pV-TCHZ correction for asymmetric parameters.

Cell lines. Cytotoxicity studies were carried out on mucoepidermoid carcinoma of human lung (NCI-H292), Human colorectal adenocarcinoma (HT-29) and Human promyelocytic

leukemia cells (HL-60) cell lines. The cells were maintained in DMEM (Dulbecco's modified Eagle's medium) (Sigma), with the exception of the HL-60 cell line that was grown in RPMI 1640. All these cell lines were supplemented with 10% fetal calf serum (GIBCO), 1% antibiotic solution (penicillin 1000 IU mL^{-1} + streptomycin 250 mg mL^{-1}) and 1% L-glutamine (200 mM).

Incorporation of doxorubicin. The doxorubicin loading was performed by introducing, under stirring for 1 d, 100 mg of the dehydrated powder material in 10 ml aqueous solution (Milli-Q water) containing 300 mg of doxorubicin as described by Hocajada and co-workers.[23] After drug insertion, the remaining Milli-Q water was removed by freeze-drying for 2 d. The amount of doxorubicin adsorbed into the porous solids was estimated by FTIR, TGA, XRPD, and UV-vis spectroscopy.

Cytotoxic activity. The cytotoxicity tests were performed on the NCI, HT29 and HL-60 cell lines, and were maintained in accordance with the protocol established by the Cell Culture Laboratory of the Department of Antibiotics, UFPE.[47] The cytotoxicity tests were carried out using the 3-(4,5-dimethyl-2-thiazolyl)-2,5-diphenyl-2*H*-tetrazolium bromide (MTT) (Sigma Aldrich Co., St. Louis, MO/USA) reduction assay. For all experiments, tumor cells were plated in 96-well plates (10^5 cells mL^{-1} for adherent cells or 3×10^5 cells mL^{-1} for leukemia). Tested compound (0.1–25 μg mL^{-1}) dissolved in DMSO (1%) was added to each well and incubated for 72 h. Control groups received the same amount of DMSO. After 69 h of treatment, 25 μL of MTT (5 mg mL^{-1}) was added. After 3 h, the MTT-formazan product was dissolved in 100 μL of DMSO, and the absorbance was measured at 595 nm in a plate spectrophotometer. Doxorubicin (0.01–5 μg mL^{-1}) was used as the positive control. Data are presented as IC_{50} values with their 95% confidence intervals (CI 95%) obtained by nonlinear regression.

Confocal microscopy. In order to investigate the dynamics of absorption and interaction of the compounds on promyelocytic leukemia, the cells were treated with 0.03 and 5.1 mg mL^{-1} of doxorubicin and DOXO–ZIF-8, respectively. ZIF-8 (5 mg mL^{-1}) was also used to compare with DOXO–ZIF-8. Cells were grown in 96 well plates with RPMI 1640 medium supplemented with 10% serum fetal bovine (GIBCO), 1% antibiotic solution (penicillin 1000 IU mL^{-1} streptomycin + 250 mg mL^{-1}), and 1% L-glutamine (200 mM), under an atmosphere of 5% CO_2 at 37 °C and then incubated for 24 and 48 h, respectively. Then cells were collected and analyzed by confocal microscopy with laser reflection at 488 nm. Optical sections were made, and a three-dimensional reconstruction with maximum projection and topography was made by Leica Microsystems Heidelberg GmbH.

Drug loading and release profile study *in vitro*. The quantification of drug adsorbed on ZIF-8 was performed using UV-vis spectroscopy (single-beam spectrometer Cary 50/variants). This material was subjected to the centrifugation process and its supernatant was used to quantify the drug concentration. Because the system DOXO–ZIF-8 is insoluble in water, the percentage of adsorbed mass of doxorubicin was determined by performing the subtraction of the amounts of their initial and final masses used for incorporation. The quantification of doxorubicin was performed from the calibration curve of doxorubicin in water. The loading efficiency is given by eqn (1):

$$LoadingEfficiency(\%) = \frac{[Doxo_{added}](mg) - [Doxo_{remained}](mg)}{[Doxo_{added}](mg)} \times 100 \quad (1)$$

A sample of DOXO–ZIF-8 was added to a dissolution medium containing 900 ml of deionized water at 37.5 ± 0.5 °C with a stirring speed of 96 rpm until full release or within 48 h of the onset of testing.[11] A volume aliquot was collected for every 2 mL of dissolution medium. The sample was collected at different intervals during a period of 48 h.

Molecular docking calculations. A hybrid search method based on the Lamarckian genetic algorithm (LGA) implemented in the AutoDock4 software was used for the docking simulations of doxorubicin onto/into ZIF-8.[48] Atomic coordinates of the ZIF-8 structure were taken from the crystallographic structures determined at normal and high pressures in order to account for the potential flexibility of the material.[49,50] However, the conformational differences between the two crystallographic structures were not significant to result in distinct doxorubicin binding-poses during independent docking calculations. Therefore, only results obtained from docking calculations using the normal pressure crystal structure are reported here. During the conformational search, doxorubicin was fully flexible concerning its degrees of translation, orientation, and conformation with respect to the ZIF-8 structure, which was kept rigid. Each sampled conformation was evaluated and ranked according to an empirical energy function.[51] Grid maps with 126 × 126 × 126 points of dimension were calculated using AutoGrid4.[52] Coarse (grid-point spacing of 0.25 Å) and fine (grid-point spacing of 0.14 Å) sets of grid maps were used during the docking simulations in order to sample the entire ZIF-8 structure and ensure accurate estimates of host–guest interaction energies. Partial charges on doxorubicin were obtained *via ab initio* calculations employing the 6-31G* basis set using the NWChem software.[53] Partial charges on the ZIF-8 structure were taken from Rana *et al.*[54] The LGA parameters used during the conformational search were: an initial population of 50 random individuals, a maximum number of 1.5×10^6 energy evaluations, a maximum number of 27 000 generations, and mutation and crossover rates of 0.02 and 0.08, respectively. An optional elitism parameter equal to 1 was applied. A maximum of 300 iterations per local search was allowed. The lowest energy docked conformations were sorted in order of increasing energy and the root-mean-square deviation (RMSD) of each conformation was calculated and compared in order to cluster together conformations with a RMSD smaller than 1.5 Å. A detailed description of the LGA parameters and procedures employed here can be found elsewhere.[55,56]

Acknowledgements

We appreciate the financial support from the following Brazilian agencies, institutes, and networks: CNPq, CAPES, FACEPE, FAPITEC-SE, INAMI, RENAMI and nBioNet. Computational

resources were provided by CENAPAD (Centro Nacional de Processamento de Alto Desempenho) in Campinas, Brazil and the Environmental Molecular Sciences Laboratory at Pacific Northwest National Laboratory. Dr Regina Figueiredo is acknowledged for the confocal microscopy imaging.

References

1 J. R. Heath and M. E. Davis, *Annu. Rev. Med.*, 2008, **59**, 251–265.
2 M. Ferrari, *Nat. Rev. Cancer*, 2005, **5**, 161–171.
3 M. E. Davis, Z. G. Chen and D. M. Shin, *Nat. Rev. Drug Discovery*, 2008, **7**, 771–782.
4 D. Peer, J. M. Karp, S. Hong, O. C. Farokhzad, R. Margalit and R. Langer, *Nat. Nanotechnol.*, 2007, **2**, 751–760.
5 R. C. Huxford, J. D. Rocca and W. B. Lin, *Curr. Opin. Chem. Biol.*, 2010, **14**, 262–268.
6 H. Li, M. Eddaoudi, M. O'Keeffe and O. M. Yaghi, *Nature*, 1999, **402**, 276–279.
7 M. Eddaoudi, D. B. Moler, H. Li, B. Chen, T. M. Reineke, M. O'Keeffe and O. M. Yaghi, *Acc. Chem. Res.*, 2001, **34**, 319–330.
8 M. Eddaoudi, H. Li and O. M. Yaghi, *J. Am. Chem. Soc.*, 2000, **122**, 1391–1397.
9 S. L. James, *Chem. Soc. Rev.*, 2003, **32**, 276–288.
10 A. Corma, H. Garcila and F. X. Llabreés i Xamena, *Chem. Rev.*, 2010, **110**, 4606–4655.
11 A. Boultif and D. Louer, *J. Appl. Crystallogr.*, 2004, **37**, 724–731.
12 K. L. Mulfort, O. K. Farha, C. D. Malliakas, M. G. Kanatzidis and J. T. Hupp, *Chem.–Eur. J.*, 2010, **16**, 276–281.
13 O. K. Farha, C. D. Malliakas, M. G. Kanatzidis and J. T. Hupp, *J. Am. Chem. Soc.*, 2009, **132**, 950–952.
14 D. J. Tranchemontagne, J. L. Mendoza-Cortes, M. O'Keeffe and O. M. Yaghi, *Chem. Soc. Rev.*, 2009, **38**, 1257–1283.
15 D. Farrusseng, S. Aguado and C. Pinel, *Angew. Chem., Int. Ed.*, 2009, **48**, 7502–7513.
16 A. M. Shultz, O. K. Farha, J. T. Hupp and S. T. Nguyen, *J. Am. Chem. Soc.*, 2009, **131**, 4204–4205.
17 A. P. Nelson, O. K. Farha, K. L. Mulfort and J. T. Hupp, *J. Am. Chem. Soc.*, 2008, **131**, 458–460.
18 S. Natarajan and P. Mahata, *Chem. Soc. Rev.*, 2009, **38**, 2304–2318.
19 I. T. Weber, A. J. G. de Melo, M. A. D. Lucena, M. O. Rodrigues and S. Alves, *Anal. Chem.*, 2011, **83**, 4720–4723.
20 A. C. McKinlay, R. E. Morris, P. Horcajada, G. Ferey, R. Gref, P. Couvreur and C. Serre, *Angew. Chem., Int. Ed.*, 2010, **49**, 6260–6266.
21 P. Horcajada, T. Chalati, C. Serre, B. Gillet, C. Sebrie, T. Baati, J. F. Eubank, D. Heurtaux, P. Clayette, C. Kreuz, J. S. Chang, Y. K. Hwang, V. Marsaud, P. N. Bories, L. Cynober, S. Gil, G. Ferey, P. Couvreur and R. Gref, *Nat. Mater.*, 2010, **9**, 172–178.
22 P. Horcajada, C. Serre, G. Maurin, N. A. Ramsahye, F. Balas, M. Vallet-Regi, M. Sebban, F. Taulelle and G. Ferey, *J. Am. Chem. Soc.*, 2008, **130**, 6774–6780.
23 X.-C. Huang, Y.-Y. Lin, J.-P. Zhang and X.-M. Chen, *Angew. Chem., Int. Ed.*, 2006, **45**, 1557–1559.
24 K. S. Park, Z. Ni, A. P. Côté, J. Y. Choi, R. Huang, F. J. Uribe-Romo, H. K. Chae, M. O'Keeffe and O. M. Yaghi, *Proc. Natl. Acad. Sci. U. S. A.*, 2006, **103**, 10186–10191.
25 O. M. Yaghi, M. O'Keeffe, N. W. Ockwig, H. K. Chae, M. Eddaoudi and J. Kim, *Nature*, 2003, **423**, 705–714.
26 S. Keskin and S. Kızılel, *Ind. Eng. Chem. Res.*, 2011, **50**, 1799–1812.
27 C. Y. Sun, C. Qin, X. L. Wang, G. S. Yang, K. Z. Shao, Y. Q. Lan, Z. M. Su, P. Huang, C. G. Wang and E. B. Wang, *Dalton Trans.*, 2012.
28 R. R. Patil, S. A. Guhagarkar and P. V. Devarajan, *Crit. Rev. Ther. Drug Carrier Syst.*, 2008, **25**, 1–61.
29 K. S. Park, Z. Ni, A. P. Cote, J. Y. Choi, R. Huang, F. J. Uribe-Romo, H. K. Chae, M. O'Keeffe and O. M. Yaghi, *Proc. Natl. Acad. Sci. U. S. A.*, 2006, **103**, 10186–10191.
30 R. Chouhan and A. Bajpai, *J. Nanobiotechnol.*, 2009, **7**, 5.
31 P. Horcajada, C. Serre, M. Vallet-Regi, M. Sebban, F. Taulelle and G. Ferey, *Angew. Chem., Int. Ed.*, 2006, **45**, 5974–5978.
32 T. Mosmann, *J. Immunol. Methods*, 1983, **65**, 55–63.
33 P. Skehan, R. Storeng, D. Scudiero, A. Monks, J. Mcmahon, D. Vistica, J. T. Warren, H. Bokesch, S. Kenney and M. R. Boyd, *J. Natl. Cancer Inst.*, 1990, **82**, 1107–1112.
34 X. W. Dai, Z. L. Yue, M. E. Eccleston, J. Swartling, N. K. H. Slater and C. F. Kaminski, *Nanomed.: Nanotechnol., Biol. Med.*, 2008, **4**, 49–56.
35 W. Morris, C. J. Stevens, R. E. Taylor, C. Dybowski, O. M. Yaghi and M. A. Garcia-Garibay, *J. Phys. Chem. C*, 2012, **116**, 13307–13312.
36 C. O. Ania, E. Garcia-Perez, M. Haro, J. J. Gutierrez-Sevillano, T. Valdes-Solis, J. B. Parra and S. Calero, *J. Phys. Chem. Lett.*, 2012, **3**, 1159–1164.
37 D. Fairen-Jimenez, S. A. Moggach, M. T. Wharmby, P. A. Wright, S. Parsons and T. Duren, *J. Am. Chem. Soc.*, 2011, **133**, 8900–8902.
38 B. Liu, H. Shioyama, T. Akita and Q. Xu, *J. Am. Chem. Soc.*, 2008, **130**, 5390–5391.
39 H. M. Rietveld, *J. Appl. Crystallogr.*, 1969, **2**, 65–71.
40 A. C. Larson and R. B. Von Dreele, General Structure Analysis System (GSAS), Los Alamos National Laboratory Report LAUR 86-748 (1994).
41 B. H. Toby, *J. Appl. Crystallogr.*, 2001, **34**, 210–213.
42 D. W. Lewis, A. R. Ruiz-Salvador, A. Gómez, L. M. Rodriguez-Albelo, F.-X. Coudert, B. Slater, A. K. Cheetham and C. Mellot-Draznieks, *CrystEngComm*, 2009, **11**, 2272–2276.
43 M. Jarvinen, *J. Appl. Crystallogr.*, 1993, **26**, 525–531.
44 P. Thompson, D. E. Cox and J. B. Hastings, *J. Appl. Crystallogr.*, 1987, **20**, 79–83.
45 R. A. Young and P. Desai, *Archiwun Nauki o Materialach*, 1989, **10**, 71–90.
46 V. Sidey, *J. Appl. Crystallogr.*, 2004, **37**, 1013–1014.
47 M. Tim, *J. Immunol. Methods*, 1983, **65**, 55–63.
48 G. M. Morris, R. Huey, W. Lindstrom, M. F. Sanner, R. K. Belew, D. S. Goodsell and A. J. Olson, *J. Comput. Chem.*, 2009, **30**, 2785–2791.
49 D. W. Lewis, A. R. Ruiz-Salvador, A. Gomez, L. M. Rodriguez-Albelo, F.-X. Coudert, B. Slater, A. K. Cheetham and C. Mellot-Draznieks, *CrystEngComm*, 2009, 11.
50 D. Fairen-Jimenez, S. A. Moggach, M. T. Wharmby, P. A. Wright, S. Parsons and T. Duüren, *J. Am. Chem. Soc.*, 2011, **133**, 8900–8902.
51 R. Huey, G. M. Morris, A. J. Olson and D. S. Goodsell, *J. Comput. Chem.*, 2007, **28**, 1145–1152.
52 P. J. Goodford, *J. Med. Chem.*, 1985, **28**, 849–857.
53 M. Valiev, E. J. Bylaska, N. Govind, K. Kowalski, T. P. Straatsma, H. J. J. van Dam, D. Wang, J. Nieplocha, E. Apra, T. L. Windus and W. A. de Jong, *Comput. Phys. Commun.*, 2010, **181**, 1477–1489.
54 M. K. Rana, F. G. Pazzona, G. B. Suffritti and F. Demontis, *J. Chem. Theory Comput.*, 2010, **7**, 1575–1582.
55 T. A. Soares, D. S. Goodsell, R. Ferreira, A. J. Olson and J. M. Briggs, *J. Mol. Recognit.*, 2000, **13**, 146–156.
56 T. A. Soares, D. S. Goodsell, J. M. Briggs, R. Ferreira and A. J. Olson, *Biopolymers*, 1999, **50**, 319–328.

